Journal of Materials Chemistry A

Accepted Manuscript

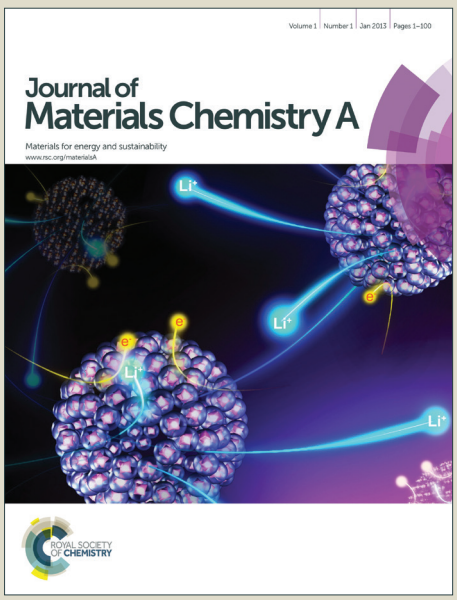

This is an *Accepted Manuscript*, which has been through the Royal Society of Chemistry peer review process and has been accepted for publication.

Accepted Manuscripts are published online shortly after acceptance, before technical editing, formatting and proof reading. Using this free service, authors can make their results available to the community, in citable form, before we publish the edited article. We will replace this *Accepted Manuscript* with the edited and formatted *Advance Article* as soon as it is available.

You can find more information about *Accepted Manuscripts* in the Information for Authors.

Please note that technical editing may introduce minor changes to the text and/or graphics, which may alter content. The journal's standard Terms & Conditions and the Ethical guidelines still apply. In no event shall the Royal Society of Chemistry be held responsible for any errors or omissions in this *Accepted Manuscript* or any consequences arising from the use of any information it contains.

ROYAL SOCIETY OF CHEMISTRY

www.rsc.org/materialsA

The table of contents

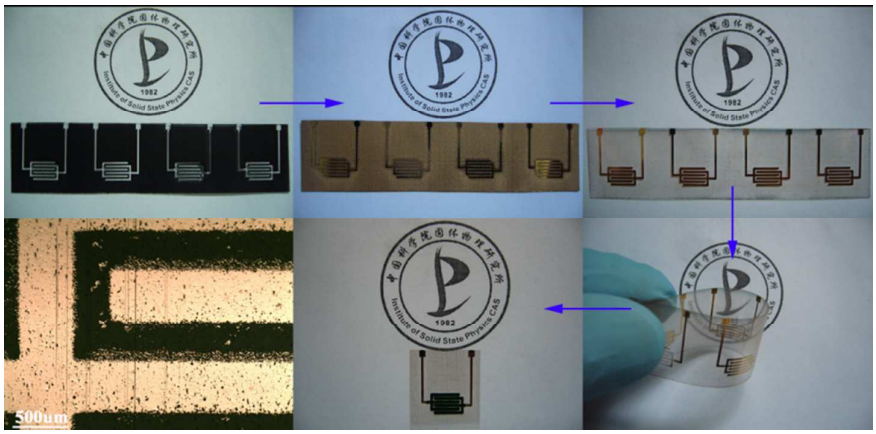

The combination of laser printing technology with in-situ electropolymerization approach enables the fabrication of flexible, in-plane, and all-solid-state micro-supercapacitors with low-cost.

Journal of Materials Chemistry A Accepted Manuscript

Cite this: DOI: 10.1039/c0xx00000x

www.rsc.org/xxxxxx

ARTICLE TYPE

Flexible, in-plane, and all-solid-state micro-supercapacitors based on printed interdigital Au/polyaniline networks hybrid electrodes on a chip

Haibo Hu,*[a] Kun Zhang,[a,b] Shuxin Li,[a] Shulin Ji[a], and Changhui Ye*[a]

Received (in XXX, XXX) Xth XXXXXXXXX 20XX, Accepted Xth XXXXXXXXX 20XX
DOI: 10.1039/b000000x

A simple and rapid fabrication method involving laser printing technology and in-situ anodic electropolymerization is introduced to fabricate interdigital Au/polyaniline network hybrid electrodes on polyethylene terephthalate films for flexible, in-plane, and all-solid-state micro-supercapacitors. The as-obtained micro-supercapacitors acquire a maximum energy density of 5.83 mWh cm^{-3} and a maximum power density of 0.45 W cm^{-3} that are both comparable to or superior to the values obtained for currently available state-of-the-art planar supercapacitors/micro-supercapacitors. In addition, the micro-supercapacitors exhibit remarkably high mechanical flexibility and show a good cycling stability, with 72.7% retention of the specific capacity after 1000 cycles. Moreover, the micro-supercapacitors can be optionally connected in series or in parallel to meet the voltage and capacity requirements for a given application. Compared to traditional fabrication approaches for flexible micro-supercapacitors with an interdigital in-plane design, the method demonstrated here does not involve complicated lithography process, toxic chemical treatments, expensive rigid template, and cumbersome fabrication of jettable and stable precursor ink, which provides a simple route for fabrication of flexible planar micro-supercapacitors with high-practicality and high-performance.

Introduction

The rapid advancement of miniaturized portable/wearable electronic equipments as well as the increasing demand for wireless and self-powered sensor networks for the development of Internet of Things has stimulated the development of flexible and all-solid-state energy storage devices with high performance.[1-5] Electrochemical capacitors, also called super-capacitors (SCs), are the state-of-the-art energy storage devices that fill the gap between the high specific energy batteries and the high specific power conventional electrostatic capacitors.[6-9] Because they can provide energy density higher by orders of magnitude than conventional electrostatic capacitors, and greater power density and longer cycling stability than batteries, SCs in thin film form are gaining increasing interest in the field of flexible and all-solid-state energy storage devices for portable/wearable electronics.[10-15]

With a few exceptions, the majority of reported flexible SCs consist of either thin film electrodes that are stacked on top of each other with a separator in between,[16-18] or symmetrical interdigital electrodes with equal inter-space arranged on a planar substrate.[19-21] While the former configuration with sandwich design is applicable to most of the electroactive materials and cost-effective for mass production, it suffers from obvious drawbacks of the possibility of short circuit and undesired position dislocation of electrodes under various application conditions.[1,13] In comparison to the former configuration, the later with in-plane design has more advantages in spite of the lower areal energy density. Firstly, flexible SCs constructed in this configuration can effectively prevent electrode short circuit and undesired position dislocation of electrodes under various application conditions. Secondly, because there is no usage of an organic binder and a polymer separator, SCs constructed in this configuration possess excellent mechanical and electrical properties. Finally, the in-plane configuration of the electrodes could facilitate fabrication and integration of the SCs. All these performances enable them to be prospective candidates for direct on-chip integration with micro-sensors and micro-electronics to be powered.[5,22] Therefore, the interdigital in-plane configuration is preferable in the fabrication of flexible SCs.[23-26]

Currently, most of the state-of-the-art flexible SCs with interdigital in-plane configuration are fabricated based on conventional lithography[20,24] or ink-jet/screen printing [21, 26, 27]. By utilization of conventional lithography, it is possible to control the fine spacing between interdigital electrodes more accurately, which may result in excellent electrochemical performance because of the decreased ion transport resistance in cells. However, lithography technique normally involves complicated lithography process, toxic chemical treatments, and harsh fabrication conditions, thus resulting in high production cost, complicated production process, and a certain degree of environmental pollution. Ink-jet and screen printing technology is a kind of simple and high-utilization method, which can accomplish the deposition and patterning in the same step, reducing material usage and process complexity. However, as it is difficult to prepare stable and jettable precursor ink, the development of ink-jet and screen printing technology in SCs fabrication is slow and only a handful of active materials have been ink-jet or screen printed. In addition, the screen printing needs to prepare expensive rigid template on-demand before printing, leading to a cumbersome fabrication process with high-cost. The limitations of these methods spur us to seek for other

Journal of Materials Chemistry A Accepted Manuscript

simple, low-cost and high-throughput method to fabricate flexible and planar all-solid-state SCs with high performance.

Herein, we introduce a method to fabricate flexible and all-solid-state micro-supercapacitors (MSCs) with planar configuration. In this method, commercial laser printers (HP LaserJet 400 M401) was used to print the interdigital circuit template on a soft and bendable polyethylene terephthalate (PET) film, into which very thin layer of gold were deposited through electron beam evaporation to form electrodes to enable effective charge transport. Then PANI nanowires network films were deposited on Au electrodes by in-situ anodic electropolymerization (AEP) of aniline monomers as the active material. A gel solution of polyvinyl alcohol (PVA) mixed with sulfuric acid (H_2SO_4) served as a solid state electrolyte. Polyaniline (PANI), as an electronically conducting polymer, has been demonstrated as a promising pseudo-capacitive electrode material in pseudo-super-capacitors because of the relatively high theoretical specific capacity,[6,28-30] environment-friendly nature, chemical stability in air, as well as low cost of the raw material.[31,32]

The MSCs fabricated with the demonstrated method can acquire an energy density of 5.83 mWh cm-3 and a power density of 0.45 W cm-3 that are both comparable to or superior to the values obtained for currently available state-of-the-art planar supercapacitors/micro-supercapacitors fabricated based on conventional lithography, or ink-jet and screen printing methods. The obtained good performance of MSCs in this work could be attributed to the following reasons: (1) The usage of interdigital in-plane configuration. There is no use any organic binders, conductive additives, and polymer separators in the fabrication of the whole device, allowing the ions to access the active material readily. (2) The unique network structure and high electrical conductivity of PANI networks can allow abundant adsorption of ions, facilitating fast intercalation/de-intercalation of active species, and provide an effective path for the transport of electrons collected by interdigital Au electrodes. (3) Accurate control of hundred-microns-scale inter-space between interdigital electrodes and width of electrodes, which results in excellent electrochemical performance because of the decreased ion transport resistance in cells. (4) Good flexibility of the in-plane configuration, rendering good cycling stability of MSCs. Moreover, our method does not involve complicated lithography process, toxic chemical treatments, or harsh fabrication conditions, dramatically simplifying the fabrication process, reducing the production cost and environmental pollution. It is possible to realize on demand design of complicated electrode layout on computer, rapid fabrication of electrodes and in-situ electrodeposition of active material, reducing material usage and process complexity. With the excellent performance, these MSCs could act as a promising candidate for portable/wearable electronics, integrated circuits and on-chip flexible energy storage systems.

Experimental

Fabrication of Au/PANI network hybrid electrodes

All chemicals were analytical grade and were used without further purification. The Au current collectors with six interdigital fingers, on that the polyaniline networks were electrodeposited, were formed through a combination of commercial laser printing and an electron beam evaporation. Firstly, interdigital-finger-like circuit template designed on a personal computer (PC) was printed on a soft, bendable and transparent PET film with common office laser printer (Figure 1a) as a mask. Then a thin film of Au (80 nm) was deposited on the printed PET film by electron beam evaporation (Figure 1b). After removal of the printed circuit template using tetrahydrofuran, symmetrical interdigital-finger-like Au electrodes (three fingers as anodes and three as cathodes, respectively) were finally produced (Figure 1c). Subsequently, active materials (PANI nanowire networks) were in-situ electrodeposited on the surface of Au layers by oxidation of aniline (0.3 M in 1 M HCl aqueous solution) through a two-step method by a conventional three-electrode system. For the first step, the seeding layer of PANI nucleated at a potential of 0.8 V for 60 s at room temperature. Then the nanowire networks grew under constant current density of 2 mA cm^{-2}. The entire preparation process is illuminated in Figure 1.

Fabrication of flexible and all-solid-state MSCs

Two copper wires were connected to the pad of each micro-electrode using silver paste to make a connection to the electrochemical instruments. Polyvinyl alcohol (PVA)/sulfuric acid (H_2SO_4) electrolyte was prepared by adding PVA power (6 g) into H_2SO_4 aqueous solution (6 g H_2SO_4 into 60 ml deionized water). The whole mixture was heated to 85 °C under vigorous stirring until the solution became clear. After cooling down, the gel solution was drop-cast to the surface of Au/PANI network hybrid microelectrodes. After the PVA/H_2SO_4 gel being solidified, the preparation of the MSCs was finished.

Sample characterization

The morphology of Au/PANI network hybrid electrodes was characterized by scanning electron microscopy (SEM; JSM-6700M). Fourier transform infrared spectrum (FT-IR) was obtained using a Magna-IR 750 spectrometer in the range of 700-1400 cm^{-1} with a resolution of 4 cm^{-1}. Raman spectrum was taken on a LABRAM-HR confocal laser micro-Raman spectrometer using an Ar+ laser with the 514.5-nm line at room temperature. Cyclic voltammetry (CV), electrochemical impedance spectroscopy (EIS), and galvanostatic charge-discharge (GCD) measurements of MSCs were carried out on an electrochemical workstation (IM6ex, Zahner). Impedance spectroscopy measurements were performed at open circuit voltage with ±10 mV amplitude. A Panasonic DMC-FX3 digital camera was used to capture all the optical images.

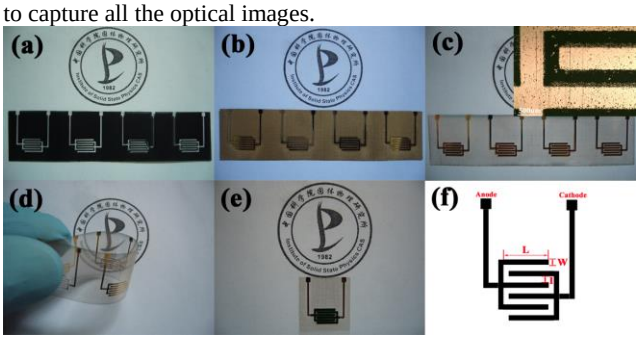

Fig.1 Schematic illustrations of the procedure for fabricating flexible MSCs with interdigital Au/PANI network hybrid electrodes on a chip, (a) flexible PET film with the printed interdigital circuit template, (b) thin layer of Au deposited on the printed interdigital circuit template, (c) and (d) obtained Au interdigital-finger-like current collectors on the PET film after removal of the printed circuit template, (e) as-obtained interdigital Au/PANI network hybrid electrodes on a chip, (f) schematic diagram of the symmetric micro-supercapacitor with 6-interdigital fingers. Inset in (c) shows the optical microscopy of Au interdigital-finger-like current collectors.

Results and discussion

The overall fabrication procedure of the flexible, in-plane, and all-solid-state MSCs with printed interdigital Au/PANI network hybrid electrodes is illustrated in Figure 1. PET film is used as the substrate, which shows excellent flexibility (Figure 1d). In

Journal of Materials Chemistry A Accepted Manuscript

This journal is © The Royal Society of Chemistry [year]

addition, PET is corrosion-resistant in the aqueous electrolytes, which is beneficial for improving the lifetime of the devices. The deposited thin layer of Au by electron beam evaporation was used as current collector for the flexible MSCs. Figure 1c is an optical photograph of the as-prepared Au interdigital-finger-like current collectors and the inset shows the photograph, which exhibits a well-defined shape and sharp boundaries. The sheet resistance of the as-obtained Au interdigital-finger-like current collectors was measured to be ~ 5.0 Ω sq^{-1}, demonstrating their excellent electrical conductivity. These results show that the approach allows ready access to the construction of delicate and high-quality electrodes. In this work, the width (W) of each interdigital finger is set to a constant value of 500 μm utilizing simple software on a PC. The inter-space (I) between interdigital fingers is designed to 300 μm, 600 μm, and 900 μm, respectively, to investigate the relation between electrochemical performance and the inter-space (defined as 300-MSC, 600-MSC, and 900-MSC, respectively). However, due to the limitation of printing precision of commercial laser printers, the width of each interdigital finger and inter-space between them are only kept for an average value of 478/330 μm, 513/622 μm, and 517/912 μm in the actual printing, respectively, containing a printer error relative to the set printing parameters. The detailed set and actual printing parameters of designed interdigital micro-electrodes are listed in the Table S1. Based on our experimental results, the printing precision of several hundreds of micrometers (≥ 300 μm) can be achieved with the commercial laser printers (HP LaserJet 400 M401). If the printing parameter is set smaller, the actual printing value will contain bigger printing errors and the print quality will also deteriorate. Figure 1f is the schematic circuit diagram of a MSC unit with 6-interdigital fingers.

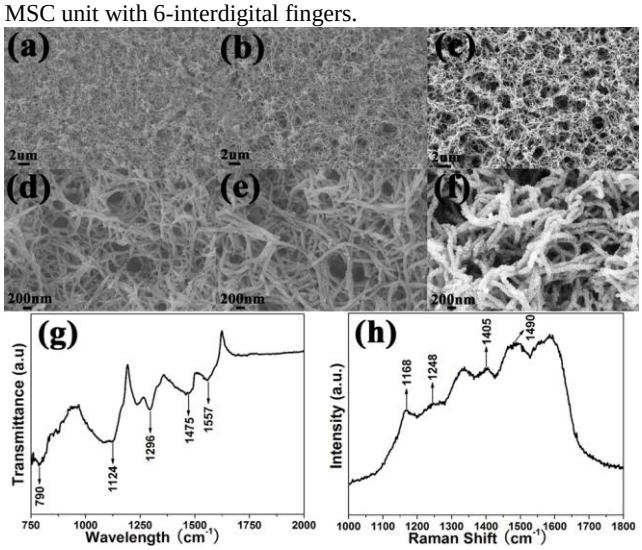

Fig.2 SEM images for PANI networks on interdigital Au electrodes grown within different deposition time, (a), (d) 120 s; (b), (e) 210 s, and (c), (f) 300 s; (g) Fourier transform infrared spectra and (h) Raman spectra for the as-deposited PANI networks on Au interdigital electrodes grown with 300 s deposition time.

As reported previously, conducting polymer nanowires are ideal electrode materials for SCs because of their large capacitance and their capability to charge and discharge at high rate.[33,34] Therefore, PANI nanowire network was selected as electrode material. Figure 1e shows the as-obtained MSCs with interdigital Au/polyaniline network hybrid electrodes that consist of 6 interdigital fingers as electrodes (three fingers as anodes and three as cathodes, respectively). While the bare interdigital Au current collectors show a shining golden yellow color (Figure 1c), the samples become dark-green after deposition of PANI (Figure 1e). SEM images of electrodeposited PANI nanowire networks on the surface of Au layers were shown in Figure 2. We can see that PANI nanowires with a diameter of dozens of nanometer to about one hundred nanometer are tangled and twisted with each other, forming films on Au current collectors. Moreover, the morphology of PANI nanowires evolved with deposition time (Figure 2a, 2d, and 2g for 120 s; Figure 2b, 2e and 2h for 210 s; Figure 2c, 2f, and 2i for 300 s; defined as MSC-120s, MSC-210s, and MSC-300s, respectively). Along with the increase of the deposition time, the diameter of PANI nanowires tended to increase and these PANI nanowires gradually formed uniform and porous network on Au-coated current collectors (Figure 2c). This special structure is beneficial for the uptake of electrolyte, acting as electrolyte reservoirs to facilitate ion transport between PANI and electrolyte.[11] The surface chemical composition of the interdigital Au/PANI network hybrid electrode was further probed by Fourier transform infrared (FTIR) and Raman spectra. In Figure 2g, the bands at 1557 and 1475 cm^{-1} corresponds to C=C stretching vibrations of quinoid and benzenoid rings, respectively. Furthermore, the band of aromatic C−N, C=N, and C−H stretching vibration at 1296, 1124, and 790 cm^{-1} can be recognized clearly, respectively.[35,36] The result illustrates the presence of PANI characteristic vibrations. In Raman spectrum (Figure 2h), four peaks are observed at about 1168, 1248, 1405, and 1490 cm^{-1}, that could be attributed to C–H bending of quinoid ring, C–H bending of the benzenoid ring, phenazine like units, and C=N stretching of the quinoid ring of PANI, respectively.[37] These all indicate that PANI had been successfully deposited on the surface of Au current collectors.

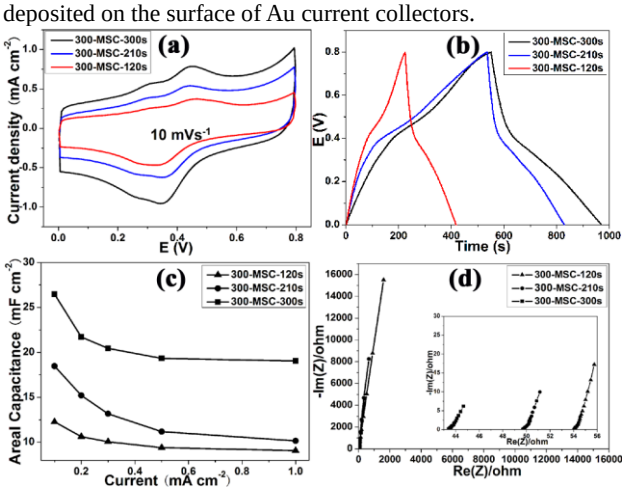

Fig.3 Electrochemical behaviors of 300-MSC-120s, 300-MSC-210s, and 300-MSC-300s: (a) Cyclic voltammetry at a scan rate of 10 mV s^{-1}; (b) Galvanostatic charge–discharge curves in the voltage range between 0 and 0.8 V at a fixed current density of 0.1 mA cm^{-2}; (c) areal capacitance plots; and (d) Nyquist plots with a frequency loop from 100 KHz to 10 mHz using perturbation amplitude of 10 mV at the open circuit potential (inset shows an enlarged curve at a high-frequency region).

Due to the use of PET as the substrate material which has no electroactivity, gram capacitance does not provide a suitable basis for comparison in this case. Instead, areal capacitance (mF cm^{-2}) is calculated from the charge-discharge curves according to the following equations to evaluate the charge-storage capacity of flexible MSCs.[26, 30, 40]

$$C = Q/\Delta E = I\Delta t/\Delta E \quad (1)$$

Journal of Materials Chemistry A Accepted Manuscript

$$Cs = C/S = I\Delta t/S\Delta E \quad (2)$$

where C is the total capacitance, Q is the total charge, I is the discharge current, Δt is the discharge time, ΔE is the potential window during the discharge process after IR drop, and S is the total surface of the positive and negative Au/polyaniline network hybrid electrodes. We firstly used the 300-MSCs with different PANI deposition time to investigate the relation between electrochemical performance and deposition time. Figure 3a shows the CV results of the as-prepared 300-MSC-120s, 300-MSC-210s, and 300-MSC-300s in the potential window of 0-0.8 V at a sweeping rate of 10 mV s^{-1}. Two pairs of distinct peaks were observed due to the redox transition of PANI networks, demonstrating a typical behavior of pseudo-capacitive super-capacitors. As shown in Figure 3a, 300-MSC-300s showed larger current density compared to 300-MSC-210s and 300-MSC-120s at the same scan rate, indicating enhanced capacitance of Au/PANI network hybrid electrodes with the increase of deposition time. Figure 3b shows the GCD curves of 300-MSCs with different PANI deposition time. It can be observed that the charge and discharge time of 300-MSCs increased with PANI deposition time from 120 to 300 s, also indicating the enhanced capacitance of 300-MSC-300s compared to 300-MSC-210s and 300-MSC-120s. The calculated areal capacitance of 300-MSCs with different PANI deposition time from GCD curves with respect to different discharge current density was plotted in Figure 3c. As can be seen from Figure 3c, 300-MSC-300s had larger areal capacitance compared to 300-MSC-210s and 300-MSC-120s, which can be attributed to an increase of the mass loading of PANI and the gradual formation of PANI networks with deposition time. However, longer deposition time of PANI will cause the possible short circuit due to the lateral growth of PANI nanowires, which will deteriorate the performance of the MSCs. The enhanced electrochemical performance of 300-MSC-300s was further confirmed by EIS measurements from 100 KHz to 10 mHz. The intercept of the Nyquist curve with the real axis at high frequencies represents the equivalent series resistance of the device with two-electrode.[19,23] As observed in the inset in Figure 3d, due to the increase of the PANI fiber diameter and the formation of perfect PANI networks with the deposition time, 300-MSC-300s shows a smaller intrinsic resistance than that of 300-MSCs-210s and 300-MSC-120s. This is of great importance since less energy and less power will be wasted to produce unwanted heat during the charge-discharge processes.

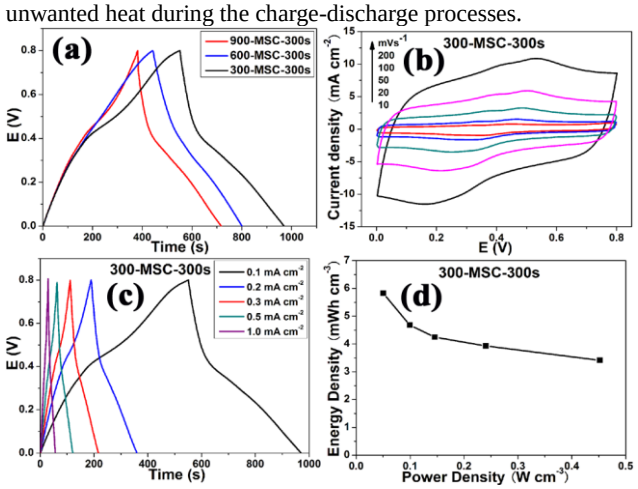

Fig.4 (a) Galvanostatic charge-discharge curves of MSC-300s with different inter-space (300, 600, and 900 μm) in the voltage range between 0 and 0.8 V at a constant current of 0.1 mA cm^{-2}; (b) Cyclic voltammetry curves of 300-MSC-300s at scan rates from 10 to 200 mV s^{-1}. (c) Galvanostatic charge-discharge curves of 300-MSC-300s in the voltage range between 0 and 0.8 V at various current densities. (d) Ragone plot of 300-MSC-300s.

Under the same PANI deposition time (300 s), MSCs-300s with different inter-space (300, 600, and 900 μm) were further used to investigate the relation between electrochemical performance and inter-space (defined as 300-MSC-300s, 600-MSC-300s, and 900-MSC-300s, respectively). Figure 4a exhibits GCD curves of MSCs-300s with different inter-space at a constant current density of 0.01 mA cm^{-2}. The triangle-shaped GCD curves of galvanostatic demonstrated a typical behavior of super-capacitors. In addition, 300-MSC-300s showed a longer charge-discharge time compared to 600-MSC-300s and 900-MSC-300s. At 0.1 mA cm^{-2}, the areal capacitance of 300-MSC-300s calculated according to GCD curves reached c.a. 26.49 mF cm^{-2}, which is significantly higher than those of 600-MSC-300s (c.a.20.93 mF cm^{-2}) and 900-MSC-300s (c.a.20.44 mF cm^{-2}). According to previous reports, the smaller line-width will reduce the transport path of ions and charges, which is conductive to complete usage of active materials and improvement of rate capability.[24,38] Since the same electrodes (the same width of each interdigited finger and the same PANI deposition time) were utilized for all MSCs-300s in this study, an increase in inter-space between two electrodes must result in the increase of pathway for ion transport from one electrode to the counted electrode. Thus, areal capacitance decreased as the inter-space between the interdigited finger line-width increased. Due to the limitation of printing precision of commercial laser printer, we are not able to further shorten the inter-space between two electrodes to improve the capacitance. However, we have reasons to believe that if better printers are used in the protocol, the smaller inter-space between two electrodes can be achieved, which could further enhance the performance of MSCs.

Based on above results, 300-MSC-300s was selected as the typical flexible, in-plane, and all-solid-state MSCs to conduct further electrical property tests. Figure S1 is the cross-sectional SEM image of the interdigital Au/PANI network hybrid electrodes of 300-MSC-300s, where the height of PANI network layer was ~ 3.95 μm. Figure 4b and S2 show the CV results of 300-MSC-300s in the potential window of 0-0.8 V, with a wide range of scan rates: from 10 mV s^{-1} to 0.5 V s^{-1}. As the scan rate increases from 10 to 200 mV s^{-1}, the peak current density increases and CV curves show a typical pseudo-capacitive shape (Figure 4b). When the scan rate further increases from 200 to 500 mV s^{-1}, the peak current density continues to increase but the shape deviates from that of an ideal pseudo-capacitance (Figure S2). Figure 4c shows the GCD curves of the 300-MSC-300s in the voltage range between 0 and 0.8 V at different current densities. Both the symmetrical and linear profile of the charge and discharge curves indicated the good capacitive performance of the all-solid-state device. At 0.1 mA cm^{-2}, the areal and volumetric capacitance of 300-MSC-300s reached c.a. 26.49 mF cm^{-2} and 67.06 F cm^{-3}, both of these data are comparable to or superior to the values obtained for other currently available SCs/MSCs with interdigital in-plane configuration.[20,22,25,26,38] As the current density increases, the areal and volumetric capacitances gradually decrease to 19.05 mF cm^{-2} and 48.23 F cm^{-3} at a high current density of 1.0 mA cm^{-2}, respectively, achieving a high capacitance retention ratio of c.a. 71.9%. These observations indicate that 300-MSC-300s possesses a fast rate capability. The discharged volumetric energy density W (Wh cm^{3}) and power density P (W cm^{3}) of the flexible and all-solid-state MSCs were the crucial parameters for practical applications, and can be calculated from GCD curves according to the following equations[25-27, 30, 40]

Journal of Materials Chemistry A Accepted Manuscript

This journal is © The Royal Society of Chemistry [year]

$$W = 0.5C(\Delta E)^2 / 3600V \quad (3)$$

$$P = W / \Delta t V \quad (4)$$

where C is the total capacitance of the device, which can be achieved through Equation 1, ΔE is the operating voltage (the applied voltage minus the voltage caused by iR drop) of the device, V is the total volume of the positive and negative Au/polyaniline network hybrid electrodes and Δt is the discharging time. Figure 4d is the Ragone plot showing the volumetric energy density with respect to the volumetric power density of the fabricated 300-MSC-300s. As shown in Figure 4d, the as-fabricated flexible and all-solid-state 300-MSC-300s with Au/polyaniline network hybrid electrodes exhibits a maximum volumetric energy density of 5.83 mWh cm^{-3}, which is higher than that reported for the planar micro-supercapacitors based on hybrid MnOx/Au electrodes (1.75 mWh cm^{-3}),[20] graphene oxide based in-plane supercapacitors (0.43 mWh cm^{-3}),[22] interdigitated multi-walled carbon nanotubes electrodes based supercapacitors (0.4 mWh cm^{-3}),[38] and graphite/polyaniline-paper electrodes based supercapacitors (0.32 mWh cm^{-3}).[41] The maximum volumetric power density is 0.45 W cm^{-3}, which is higher than that of planar micro-supercapacitors based on hybrid MnOx/Au electrodes (0.079 W cm^{-3}),[20] interdigitated multi-walled carbon nanotubes electrodes based supercapacitors (0.19 W cm^{-3}),[38] and graphite/polyaniline-paper electrodes based supercapacitors (0.054 W cm^{-3}).[41] The performance of the as-presented MSCs could still be improved further with a proper design of fine interdigited electrodes with a better printer, and the work is underway.

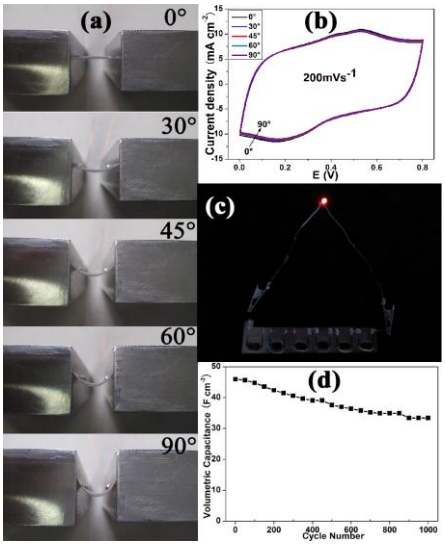

Fig.5 (a) The photographs of the flexible, in-plane, and all-solid-state 300-MSC-300s at five bending states with bending angle of 0°, 30°, 45°, 60° and 90°; (b) Cyclic voltammetry curves of the 300-MSC-300s at the five bending states; (c) The photograph of six 300-MSC-300s connected in series to light a red LED; (d) The long-term cycling stability of 300-MSC-300s, measured at a high scan rate of 200 mV s^{-1}.

The as-obtained in-plane MSCs also possess excellent flexibility. As shown in Figure 5a, the as-prepared 300-MSC-300s is highly flexible, which can be bent to 90° at least, remaining the CV curves nearly unchanged at a high scan rate of 200 mV s^{-1} (Figure 5b). In addition, we connected six 300-MSC-300s in series to light a red light-emitting diode (LED) (Figure 5c), demonstrating its practical application in flexible energy storage. As a potential energy storage device, the long-term stability of MSCs must be examined. Therefore, the cycling performance of 300-MSC-300s was further tested with cyclic voltammetry at a high scan rate of 200 mV s^{-1} over 1000 cycles and the result was shown in Figure 5d. Although the result showed that the capacitance of 300-MSC-300s deteriorated gradually, it still retained about 72.7% after 1000 cycles with respect to the first cycle.

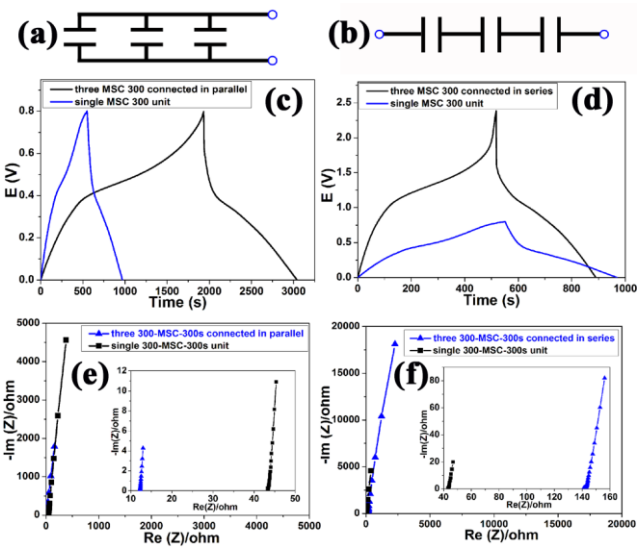

Fig.6 Circuit diagram of three 300-MSC-300s units connected (a) in parallel and (b) in series; (c) Galvanostatic charge/discharge curves for single 300-MSC-300s unit and three 300-MSC-300s units connected in parallel and (d) in series at the same constant current density of 0.1 mA cm^{-2}; Nyquist plots of (e) three 300-MSC-300s connected in parallel and (f) in series with a frequency loop from 100 KHz to 10 mHz using perturbation amplitude of 10 mV at the open circuit potential. Insets in (e) and (f) are enlarged views at high-frequency regions.

In consideration of real-world applications of supercapacitors, it is necessary to connect supercapacitors in series and/or in parallel to increase operating voltage and capacity in certain situations. Therefore, the performance of integrated SCs pack with three 300-MSC-300s connected in parallel and series was further tested. Figure 6a and b illustrate the schematics of three 300-MSC-300s units connected in parallel and series. As shown in Figure 6c of GCD curves of single 300-MSC-300s unit and three 300-MSC-300s units connected in parallel at the same constant current of 0.1 mA cm^{-2}, the runtime of the electrochemical capacitor pack (three parallel-connected 300-MSC-300s units) increases by a factor of three compared to single 300-MSC-300s unit. The calculated capacitance of the electrochemical capacitor pack and single 300-MSC-300s unit was 17.1 and 6.0 mF, respectively, which revealed that the MSCs roughly obeyed the basic rule of parallel connections. Therefore, putting MSCs together in parallel can easily enhance the capacity, while the operating voltage remains the same. The intercept of the Nyquist curve with the real axis at high frequencies represents the equivalent series resistance of the device.[20,24] As observed in Figure 6c, the inner resistance of three parallel-connected 300-MSC-300s units was only about a third of single MSC 300 unit, which can explain the above result. Figure 6d exhibits the GC curves of single 300-MSC-300s unit and three units connected in serial at the same constant current of 0.1 mA cm^{-2}. As shown in

Journal of Materials Chemistry A Accepted Manuscript

Figure 6d, adding electrochemical capacitors together in a serial string can effectively increase the voltage. However, because the inner resistance was superimposed after MSC units connected in series (Figure 6f), the capacity of three 300-MSC-300s units connected in series (2.5 mF) was reduced slightly compared with the single 300-MSC-300s unit (6.0 mF), also roughly confirming to the theorem of series connections of capacitors. The above results clearly indicate that as-obtained MSCs can be optionally connected in series or in parallel to meet the voltage and capacity requirements for a given application.

Conclusions

In summary, flexible, in-plane, and all-solid-state micro-supercapacitors on the basis of printed interdigital Au/polyaniline networks hybrid electrodes are successfully fabricated with a simple method. By the combination of laser printing technology and in-situ anodic electropolymerization, our method allows for the fabrication of planar MSCs without the use of traditional time-consuming and labor-intensive lithography and ink-jet/screen printing that are often used in the fabrication of MSCs with interdigital in-plane configuration. With this method, the fabricated MSCs exhibits a maximum energy density of 5.83 mWh cm^{-3} and a maximum power density of 0.45 W cm^{-3} that are both comparable to or superior to the values obtained for currently available state-of-the-art in-plane SCs/MSCs fabricated with traditional approaches. In addition, MSCs in this work possess remarkably high mechanical flexibility and show a good cycling stability, with 72.7% retention of the specific capacity after 1000 cycles. Moreover, the devices can be optionally connected in series or in parallel to meet the voltage and capacity requirements for a given application. The demonstration of the unique method for flexible, in-plane, and all-solid-state MSCs would open up new opportunities for energy storage and flexible/wearable electronics.

Acknowledgments

This work was supported by National Basic Research Program of China (973 Program, Grant No. 2011CB302103), National Natural Science Foundation of China (Grant No. 11274308 and 21401202), and the Hundred Talent Program of the Chinese Academy of Sciences.

Notes and references

[a] *Anhui Key Laboratory of Nanomaterials and Technology, and Key Laboratory of Materials Physics, Institute of Solid State Physics, Chinese Academy of Sciences, Hefei 230031, China. Telephone: +86-551-65595629; Fax: +86-551-65591434; E-mail: chye@issp.ac.cn; haibohu@issp.ac.cn*

[b] *School of Materials Science and Engineering, Hefei University of Technology, Hefei 230039, China.*

† Electronic Supplementary Information (ESI) available: [The detailed printing parameter of designed micro-electrodes of MSCs with different inter-space, the cross-sectional SEM image of PANI networks on interdigital Au electrodes grown within 300s, and the cyclic voltammetry curves of 300-MSC-300s at a high scan rate of 500 mV s^{-1}.] See DOI: 10.1039/b000000x/

1 M. Beidaghi and Y. Gogotsi, *Energy Environ. Sci*., 2014, **7**, 867-884.
2 X. H. Lu, M. H. Yu, G. M. Wang, Y. X. Tong and Y. Li, *Energy Environ. Sci*., 2014, **7**, 2160-2181.
3 Z. L. Wang, *Adv. Mater.*, 2012, **24**, 280-285.
4 X. Y. Lang, A. Hirata, T. Fujita and M. W. Chen, *Nat. Nanotechnol.*, 2011, **6**, 232-236.
5 J. Chmiola, C. Largeot, P. L. Taberna, P. Simon and Y. Gogotsi, *Science*, 2010, **328**, 480-483.
6 P. Simon and Y. Gogotsi, *Nat. Mater.*, 2008, **7**, 845-854.
7 J. R. Miller and P. Simon, *Science*, 2008, **321**, 651-652.
8 X. H. Lu, T. Zhai, X. H. Zhang, Y. Q. Shen, L. Y. Yuan, B. Hu, L. Gong, J. Chen, Y. H. Gao, J. Zhou, Y. X. Tong and Z. L. Wang, *Adv. Mater.*, 2012, **24**, 938-944.
9 C. Zhou,Y. W. Zhang, Y. Y. Li and J. P. Liu, *Nano Lett*., 2013, **13**, 2078-2085.
10 L. Y. Yuan, B. Yao, B. Hu, K. F. Huo, W. Chen and J. Zhou, *Energy Environ. Sci*., 2013, **6**, 470-476.
11 Y. M. He, W. J. Chen, X. D. Li, Z. X. Zhang, J. C. Fu, C. H. Zhao and E. Q. Xie, *ACS Nano*, 2013, **7**, 174-182.
12 L. Y. Yuan, X. Xiao, T. P. Ding, J. W. Zhong, X. H. Zhang, Y. Shen, B. Hu, Y. H. Huang, J. Zhou and Z. L. Wang, *Angew. Chem. Int. Ed.*, 2012, **51**, 4934-4938.
13 F. H. Meng and Yi Ding, *Adv. Mater*., 2011, **23**, 4098-4102.
14 Z. Weng, Y. Su, D. W. Wang, F. Li, J. H. Du and H. M. Cheng, *Adv. Energy Mater*., 2011, **1**, 917-922.
15 D. W. Wang, F. Li, J. P. Zhao, W. C. Ren, Z. G. Chen, J. Tan, Z. S. Wu, I. Gentle, G. Q. Lu and H. M. Cheng, *ACS Nano*, 2009, **3**, 1745-1752.
16 L. Y. Yuan, X. H. Lu, X. Xiao, T. Zhai, J. J. Dai, F. C. Zhang, B. Hu, X. Wang, L. Gong, J. Chen, C. G. Hu, Y. X. Tong, J. Zhou and Z. L. Wang, *ACS Nano*, 2012, **6**, 656-661.
17 C. Z. Meng, C. H. Liu, L. Z. Chen, C. H. Hu and S. S. Fan, *Nano Lett*., 2010, **10**, 4025-4031.
18 X. H. Lu, G. M. Wang, T. Zhai, M. H. Yu, S. L. Xie, Y. C. Ling, C. L. Liang, Y. X. Tong and Y. Li, *Nano Lett.*, 2012, **12**, 5376-5381.
19 D. Pech, M. Brunet, H. Durou, P. Huang,V. Mochalin, Y. Gogotsi, P. L. Taberna and P. Simon, *Nat. Nanotechnol*., 2011, **5**, 651-654.
20 W. P. Si, C. L. Yan, Y. Chen, S. Oswald, L. Y. Han and O. G. Schmidt, *Energy Environ. Sci*., 2013, **6**, 3218-3223.
21 D. Pech, M. Brunet, P. L. Taberna, P. Simon, N. Fabre, F. Mesnilgrente, V. Conédéra and H. Durou, *J. Power Sources*, 2010, **195**, 1266-1269.
22 W. Gao, N. Singh, L. Song, Z. Liu, A. Reddy, L. J. Ci, R. Vajtai, Q. Zhang, B. Q. Wei and P. M. Ajayan, *Nat. Nanotechnol.*, 2011, **6**, 496-500.
23 M. F. El-Kady and R. B. Kaner, *Nat.* Commun., 2013, **4**, 1475-1483.
24 K. Wang, W. J. Zou, B. G. Quan, A. F. Yu, H. P. Wu, P. Jiang and Z. X. Wei, *Adv. Energy Mater*., 2011, **1**, 1068-1072.
25 B. Hsia, J. Marschewski, S. Wang, J. B. In, C. Carraro, D. Poulikakos, C. P. Grigoropoulos and R. Maboudian, *Nanotechnology*, 2014, **25**, 055401-055410.
26 Y. Wang, Y. M. Shi, C. X. Zhao, J. I. Wong, X. W. Sun and H. Y. Yang, *Nanotechnology*, 2014, **25**, 094010-094018.
27 S. Shi, C. J. Xu, C. Yang, Y. Y. Chen, J. J. Liu and F. Y. Kang, *Sci. Rep.*, 2013, **3**, 2598.
28 Y. G. Wang and Y. Y. Xia, *Adv. Mater*., 2013, **25**, 5336-5342.
29 J. R. Miller, R. A. Outlaw and B. C. Holloway, *Science*, 2010, **329**, 1637-1639.
30 C. Guan, X. L. Li, Z. L. Wang, X. H. Cao, C. Soci, H. Zhang and H. J. Fan, *Adv. Mater*., 2012, **24**, 4186-4190.
31 K. Wang, H. P. Wu, Y. N. Meng and Z. X. Wei, *Small*, 2014, **10**, 14-31.
32 L. Nyholm, G. Nyström, A. Mihranyan and M. Strømme, *Adv. Mater*., 2011, **23**, 3751-3769.
33 Z. G. Yin and Q. D. Zheng, *Adv. Energy Adv. Mater*., 2012, **2**,179-218.
34 S. Il Cho and S. B. Lee, *Acc. Chem. Res.*, 2008, **41**, 699-707.
35 Z. X. Wei and M. X. Wan, *Adv. Mater*., 2002, **14**, 1314-1317.

Journal of Materials Chemistry A Accepted Manuscript

This journal is © The Royal Society of Chemistry [year]

36 Y. Yang and W. Yang, *Polym. Adv. Technol*., 2005, **16**, 24-31.
37 Z. Niu, P. Luan, Q. Shao, H. Dong, J. Li, J. Chen, D. Zhao, L. Cai, W. Zhou, X. Chen and S. Xie, *Energy Environ. Sci*., 2012, **5**, 8726-8733.
38 S. K. Kim, H. J. Koo, A. Lee and P. V. Braun, *Adv. Mater*., 2014, **26**, 5108-5112.
39 H. Y. Jung, M. B. Karimi, M. G. Hahm, P. M. Ajayan and Y. J. Jung, *Sci. Rep*., 2012, **2**, 773-778.
40 X. Xiao, X. Peng, H.Y. Jin, T. Q. Li, C. C Zhang, B. Gao, B. Hu, K. F. Huo and J. Zhou, *Adv. Mater*., 2013, **25**, 5091-5097.
41 B. Yao, L. Y. Yuan, X. Xiao, J. Zhang, Y. Y. Qi, J. Zhou, J. Zhou, B. Hu and W. Chen, *Nano Energy*, 2013, **2**, 1071-1078.

Journal of Materials Chemistry A Accepted Manuscript